ACS APPLIED MATERIALS & INTERFACES

Research Article

www.acsami.org

Tandem and Triple-Junction Polymer:Nanocrystal Hybrid Solar Cells Consisting of Identical Subcells

Haipeng Lu, Andrew N. Bartynski, Matthew J. Greaney, Mark E. Thompson, and Richard L. Brutchey*

Department of Chemistry and the Center for Energy Nanoscience, University of Southern California, Los Angeles, California 90089-0744, United States

Supporting Information

ABSTRACT: Tandem and triple-junction polymer:nanocrystal hybrid solar cells with identical subcells based on P3HT:CdSe nanocrystal bulk heterojunctions (BHJs) are reported for the first time showing 2-fold and 3-fold increases of open-circuit voltage (V_{OC}), respectively, relative to the single-junction cell. A combination of nanocrystalline ZnO and pH-neutral PEDOT:PSS is used as the interconnecting layer, and the thicknesses of subcells are optimized with the guidance of optical simulations. As a result, the average power conversion efficiency (PCE) exhibits a significant increase from 2.0% (V_{OC} = 0.57 V) in single-junction devices to 2.7% (champion 3.1%, V_{OC} = 1.28 V) in tandem devices and 2.3% (V_{OC} = 1.98 V) in triple-junction devices.

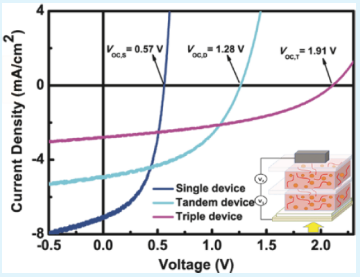

KEYWORDS: *tandem solar cell, hybrid solar cell, P3HT, CdSe, optical simulation*

I. INTRODUCTION

Polymer:nanocrystal hybrid solar cells are receiving renewed attention because of the potential they offer in combining beneficial properties of both the organic and inorganic phases.[1,2] In place of the commonly employed fullerenes, inorganic semiconductor nanocrystals can be used as alternate electron acceptors that take advantage of their intrinsically higher electron mobilities, broad and tunable absorption at energies above the band edge, and higher dielectric constants.[3−5] With this in mind, the power conversion efficiency (PCE) of polymer:nanocrystal hybrid solar cells has improved to >5%[6,7] over the past year. Proven strategies for increasing the PCE include changing the nanocrystal size and shape,[8−10] ligand engineering,[11−14] and postfilm deposition treatments (e.g., ligand exchange via dip-coating,[6,15] solvent−vapor annealing[16]). Despite these performance gains, the PCEs of polymer:nanocrystal hybrid solar cells still lag behind their all-organic counterparts. Earlier studies have shown that the main reasons for poor device performance in hybrid solar cells are low absorption (resulting from thin absorber layers) and limited charge separation efficiency resulting from the trap-mediated recombination as well as low carrier mobility.[17−19] One potential solution for increasing absorption efficiency without increasing charge recombination is applying a multi-junction device configuration.

Parallel and series multijunction device configurations have been used in organic photovoltaics (OPVs) to achieve enhanced short-circuit current and open-circuit voltage, respectively, and have thusly achieved higher PCEs than their single-junction counterparts.[20−24] When connected in series, open-circuit voltages (V_{OC}) that are the sum of the V_{OC} from individual subcells are theoretically obtained.[25] Despite the advantages of multijunction over single-junction solar cells, there is only one example of a tandem polymer:nanocrystal hybrid solar cell to the best of our knowledge. In that particular case,[26] the PCE of the tandem solar cell connected in series (η_P = 1.3%) was lower than that of the corresponding single-junction device (η_P = 1.8%), with only a 64% increase in V_{OC} relative to the single-junction cell being measured.

Herein, tandem and triple-junction polymer:nanocrystal hybrid solar cells with identical poly(3-hexylthiophene) (P3HT):CdSe nanocrystal bulk heterojunction (BHJ) subcells connected in series are reported. Interconnecting layers (ICLs) consisting of nanocrystalline ZnO and pH-neutral poly(3,4-ethylenedioxythiophene):poly(styrene sulfonic acid) (N-PEDOT:PSS) are used to successfully connect adjacent subcells. Simulations are employed to optimize the thickness of each P3HT:CdSe BHJ by maximizing the optical fields in each of the photoactive layers. As a result, tandem polymer:nanocrystal hybrid solar cells giving a 2-fold increase in V_{OC} and up to ∼50% enhancement in PCE were obtained with an increase in absorption relative to single-junction devices.

II. EXPERIMENTAL DETAILS

Materials. $CdCO_3$ (99.998% metal basis, "Puratronic" grade, Alfa Aesar), selenium (200 mesh powder, 99.999% metal basis, Alfa Aesar), tri-*n*-octylphosphine oxide (TOPO, 98%, Alfa Aesar), tri-*n*-octylphosphine (TOP, ≥97%, Strem), stearic acid (95%, Sigma-Aldrich), and pyridine (≥99.0%, "GRACS" grade, EMD) were all used as received. P3HT (≥96% rr, 65−75 kDa MW, 1.7−1.9 PDI) was purchased from Rieke Metals. Acidic A-PEDOT:PSS (Clevios PH 500, pH 1−2, percent 1−1.5) was purchased from Heraeus. Neutral N-PEDOT:PSS

Received: August 17, 2014
Accepted: September 18, 2014
Published: September 18, 2014

(high-conductivity grade, pH 5−7, percent 1.1) was purchased from Sigma-Aldrich.

Synthesis and Ligand Exchange of CdSe Nanocrystals. The synthesis and ligand exchange procedures are based on literature methods[27] and are described in detail in the Supporting Information.

Characterization. Absorption spectra were acquired on a PerkinElmer Lamba 950 spectrophotometer equipped with a 150 mm integrating sphere, using a quartz cuvette for liquid samples or a borosilicate glass microscope slide substrate for films. Thermogravimetric analysis (TGA) measurements were made on a TA Instruments TGA Q50 instrument, using sample sizes between 5 and 15 mg in an alumina crucible under a flowing nitrogen atmosphere. TGA samples were prepared by drying the colloid under flowing nitrogen at 80 °C for up to 90 min, then lightly crushing with a spatula. Film thicknesses were determined using a J. A. Woollam variable-angle spectroscopic ellipsometer equipped with a 150 W Xe arc lamp. TEM images were obtained on a JEOL JEM-2100F microscope at an operating voltage of 200 kV, equipped with a Gatan Orius CCD camera.

Single-Junction Hybrid Solar Cell Fabrication. All devices were fabricated and tested in air. Aluminum shot (Al; Alfa Aesar, 99.999%) was purchased and used as received. Patterned ITO-coated glass substrates (10 Ω cm^{-2}, Thin Film Devices, Inc.) were sequentially cleaned by sonication in tetrachloroethylene, acetone, and isopropanol followed by 30 min of UV-ozone exposure inside of an UV/Ozone ProCleaner 110 (254 nm UV light under an operation power of 60 W). A 27 nm (determined by ellipsometry) layer of A-PEDOT:PSS (Clevios PH 500, pH 1−2, percent 1−1.5, 1:1 v/v diluted by H_2O, filtered through a 0.45 μm cellulose acetate syringe filter) was spun-cast (4000 rpm, 40 s) onto the clean ITO and heated at 120 °C for 30 min under vacuum (∼5 kPa). A P3HT solution of 15 mg mL^{-1} was prepared in 1,2-dichlorobenzene by dissolution under mild heating (40−50 °C) followed by filtering through a 0.45 μm PTFE syringe filter. The pyridine-exchanged CdSe nanocrystals were dispersed in a mixed solvent of 90% 1,2-dichlorobenzene (DCB) and 10% pyridine by volume and filtered through a 0.45 μm PTFE syringe filter. To make the final blend solution, the CdSe nanocrystals (in 90% DCB, 10% pyridine) were then mixed for several hours under mild heating with the filtered P3HT solution to a final concentration of 3:24 mg mL^{-1} (P3HT:CdSe). The active layer was spun-cast at different speeds (2500, 2000, 1500, 1000, and 700 rpm, all for 50 s) onto the dried PEDOT:PSS layer to get active layer thicknesses of 42, 47, 52, 56, and 62 nm, respectively. After drying in a dark nitrogen cabinet for 20−25 min, ZnO nanocrystals (synthesized from a sol−gel method with diameters of 3−4 nm,[28] as described in the Supporting Information) dispersed in ethanol (20 mg mL^{-1}) were spun-cast on the active layer (4000 rpm, 40 s) to produce a 40 nm thick layer. The devices were then annealed at 150 °C under flowing nitrogen for 10 min. The 150 °C annealing temperature was empirically chosen to create favorable phase segregation in the BHJ; according to TGA, pyridine is not lost from the CdSe nanocrystal surface at this temperature. This annealing step was followed by loading into a high vacuum (∼2 μTorr) thermal deposition chamber (Angstrom Engineering) for deposition of 100 nm thick Al cathodes through a shadow mask at a rate of 2 Å s^{-1}. Device active areas were 4.3 mm^2 as measured by pixel mapping through a CCD-equipped optical microscope.

Tandem/Triple-Junction Hybrid Solar Cell Fabrication. The cleaning procedure for ITO substrates was identical for all devices fabricated. A 27 nm layer of A-PEDOT:PSS (Clevios PH 500, pH 1−2, percent 1−1.5, 1:1 v/v diluted by H_2O, filtered through a 0.45 μm cellulose acetate syringe filter) was spun-cast (4000 rpm, 40 s) onto the clean ITO and heated at 120 °C for 30 min under vacuum (∼5 kPa). The first active layer was spun-cast at different speeds (2000, 1500, 1000, and 700 rpm, all for 50 s) onto a dried A-PEDOT:PSS layer to get an active layer thickness of 47, 52, 56, and 62 nm, respectively. After drying in a dark nitrogen cabinet for 20−25 min, ZnO nanocrystals dispersed in ethanol (25 mg mL^{-1}) were spun-cast on the active layer (4000 rpm, 40 s) to produce a 45 nm layer. Then the device was annealed at 150 °C under flowing nitrogen for 10 min. A 9 nm layer of N-PEDOT:PSS (pH 5−7, percent 1.1, 1:2 v/v diluted by H_2O, filtered through a 0.45 μm cellulose acetate syringe filter) was spun-cast (6000 rpm, 40 s) onto the ZnO layer and heated at 120 °C for 30 min under vacuum (∼5 kPa). The second active layer was spun-cast at different speeds (2000, 1500, 1000, and 700 rpm, all for 50 s) onto the dried N-PEDOT:PSS layer. Then, the second ZnO layer (20 mg mL^{-1}) was spun-cast on the second active layer (4000 rpm, 40 s) to produce a 40 nm thick layer, and the device was annealed at 150 °C under flowing nitrogen for 10 min. To make triple-junction hybrid solar cells, the third N-PEDOT:PSS, active layer, and ZnO layers are processed in the same way as the second junction of the tandem hybrid solar cell. Finally, the devices were loaded into a high vacuum (∼2 μTorr) thermal deposition chamber (Angstrom Engineering) for deposition of 100 nm thick Al cathodes through a shadow mask at a rate of 2 Å s^{-1}.

Device Characterization. Current−density dependence on applied test voltage measurements were performed under ambient conditions using a Keithley 2400 SourceMeter (sensitivity = 100 pA) in the dark and under ASTM G173-03 spectral mismatch corrected 1000 W m^{-2} white light illumination from an AM 1.5G filtered 450 W xenon arc lamp (Newport Oriel). Chopped and filtered monochromatic light (250 Hz, 10 nm fwhm) from a Cornerstone 260 1/4 M double-grating monochromator (Newport 74125) was used in conjunction with an EG&G 7220 lock-in amplifier to perform all spectral responsivity measurements.

III. RESULTS AND DISCUSSION

The as-synthesized CdSe nanocrystals were treated with a standard pyridine exchange to help remove the insulating native ligands in order to facilitate charge transfer between the donor and acceptor phases of the BHJ.[11] The pyridine-exchanged CdSe nanocrystals used in the tandem or triple-junction hybrid solar cells discussed herein possess a diameter of 6.4 nm, as calculated from the λ_{max} of the first exciton peak at 635 nm,[27] which is in agreement with TEM analysis. Thermogravimetric analysis of the pyridine-exchanged nanocrystals shows a 5−6% mass loss up to 400 °C, which is indicative of loss of organic ligands from the surface (Figure 1).[29] This compares favorably against the as-synthesized CdSe nanocrystals (>15% mass loss up to 400 °C), suggesting some successful degree of ligand exchange.

A. Single-Junction Device Optimization. The performance of tandem/triple-junction OPVs is critically dependent on the individual subcell active layer thicknesses. As a starting point, we sought to construct single-junction P3HT:CdSe nanocrystal hybrid solar cells with an optimized active layer thickness. The single-junction hybrid solar cell was fabricated with the device configuration of ITO/PEDOT:PSS/P3HT:CdSe/ZnO/Al, with the P3HT:CdSe BHJ active layer thickness varying between 42 and 62 nm. Figure 2a shows the $I-V$ curves of single-junction devices with different active layer thicknesses under 100 mW cm^{-2} AM 1.5 G illumination, and the results are summarized in Table 1. The optimal active layer thickness was found to be 47 nm, which gives an average PCE of 1.98(0.12)%, J_{SC} = 6.95(0.33) mA cm^{-2}, V_{OC} = 0.57(0.01) V, and FF = 0.50(0.01). Active layer thicknesses less than 47 nm lead to devices with low shunt resistance (R_{SH}) and result in significant decreases in FF when compared to the optimal thickness. The thicker active layers exhibit larger R_{SH} but reduced J_{SC}, likely resulting from enhanced charge recombination owing to the relatively small exciton diffusion lengths in P3HT:CdSe BHJs.

To further investigate the active layer thickness dependence, the double-pass absorption and external quantum efficiency (EQE) of the single-junction devices with various thicknesses were measured and used to calculate the internal quantum efficiency (IQE) by dividing the EQE spectra by the absorption

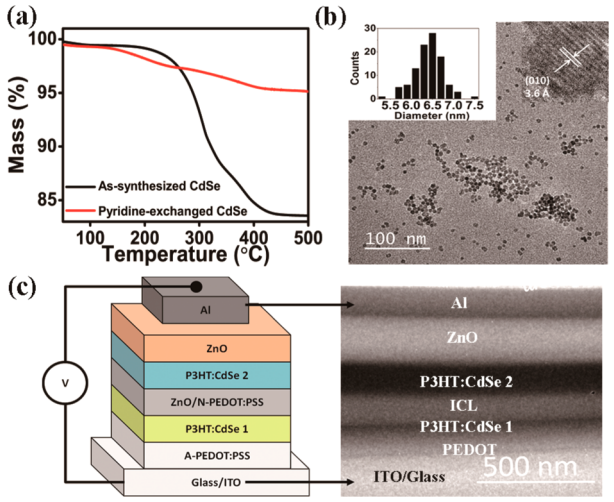

Figure 1. (a) TGA data for the as-synthesized and pyridine-exchanged CdSe nanocrystals. (b) TEM micrograph of the as-synthesized nanocrystals. Inset on the left is the size distribution, and inset on the right is a high-resolution image showing the lattice fringes of a single CdSe nanocrystal. (c) Schematic and cross-section TEM micrograph of the tandem hybrid device architecture: Glass/ITO/A-PEDOT:PSS/P3HT:CdSe(1)/ZnO/N-PEDOT:PSS/P3HT:CdSe(2)/ZnO/Al.

percentage determined from completed devices (Figures 2b and c). Photoresponse is observed out to ~700 nm, which is the absorption edge of the 6.4 nm CdSe nanocrystals used in these devices, with broadband IQE at higher energies coming from a combination of photoresponse from both P3HT and the CdSe nanocrystals. It is noteworthy to point out that the peak IQE of devices with a 47 nm (optimal) active layer thickness reaches 75%, and the values decrease with further increasing thicknesses, indicating increased charge recombination loss with thicker active layers. Thus, increasing the active layer thickness to harvest more light is not an effective approach to increase the PCE of polymer:nanocrystal hybrid solar cells, which could be potentially mediated by a tandem device architecture.

B. Tandem and Triple-Junction Devices. *B.1. Interconnecting Layer (ICL) Optimization.* The ICL is one of the most critical parameters to optimize in order to make an operable tandem hybrid solar cell. Ideally, the ICL should work as a perfect transparent ohmic contact (i.e., with no Schottky barrier). The combination of nanocrystalline ZnO and neutral N-PEDOT:PSS has been previously demonstrated to be a

Table 1. Photovoltaic Device Parameters for Single-Junction P3HT:CdSe BHJ Hybrid Solar Cells with Different Active Layer Thicknesses[a]

active layer thickness (nm)	J_{SC} (mA cm^{-2})	V_{OC} (V)	FF	PCE (%)
42	5.98 ± 0.10	0.63 ± 0.01	0.39 ± 0.12	1.66 ± 0.46
47	6.95 ± 0.33	0.57 ± 0.01	0.50 ± 0.01	1.98 ± 0.12
52	6.28 ± 0.54	0.54 ± 0.01	0.47 ± 0.02	1.61 ± 0.25
56	5.91 ± 0.07	0.54 ± 0.01	0.51 ± 0.01	1.58 ± 0.04
62	4.54 ± 0.31	0.54 ± 0.02	0.48 ± 0.01	1.17 ± 0.01

[a]The device parameters were measured under AM 1.5G illumination at 1 sun. Average numbers and the associated standard deviations were determined over a total of 10−16 devices over four separate substrates.

robust ICL for tandem/multijunction OPVs[30,31] connected in series. Here, we also observe successful serial connection when this ICL is used between two adjacent P3HT:CdSe nanocrystal BHJ subcells. It should be noted that the N-PEDOT:PSS is very important because regular, acidic A-PEDOT:PSS (pH 1−2) will partially dissolve the underlying ZnO layer. The concentrations of ZnO and N-PEDOT:PSS were both optimized empirically based on device performance. We find that 25 mg mL^{-1} of ZnO and 1:2 dilution (v/v, diluted with H_2O) of N-PEDOT:PSS gives the best device performance. Those deposition conditions result in 45 nm ZnO and 9 nm N-PEDOT:PSS layers as determined by spectroscopic ellipsometry. Thicker N-PEDOT:PSS layers decrease the overall photocurrent due to the partial light absorption by N-PEDOT:PSS, whereas thinner layers decrease the device V_{OC}, likely because of poor ohmic contact.

B.2. Tandem P3HT:CdSe Nanocrystal Subcell Thickness Optimization. Tandem hybrid solar cells with two identical subcells based on P3HT:CdSe nanocrystal BHJs were fabricated as shown in Figure 1c, with the device architecture ITO/A-PEDOT:PSS/P3HT:CdSe(1)/ZnO/N-PEDOT:PSS/P3HT:CdSe(2)/ZnO/Al. In order to guide the fabrication of the tandem solar cells, optical modeling using the transfer matrix formalism[32] was performed on relevant device architectures. Figure 3 depicts the output of simulated tandem device performance for the structure ITO/A-PEDOT:PSS (27 nm)/P3HT:CdSe(1) (x nm)/ZnO (45 nm)/N-PEDOT:PSS (9 nm)/P3HT:CdSe(2) (y nm)/ZnO (40 nm)/Al (100 nm). The simulations assume a constant IQE and are meant to focus experimental efforts and are not an absolute predictor of device performance. As a result of the optical cavity created by the

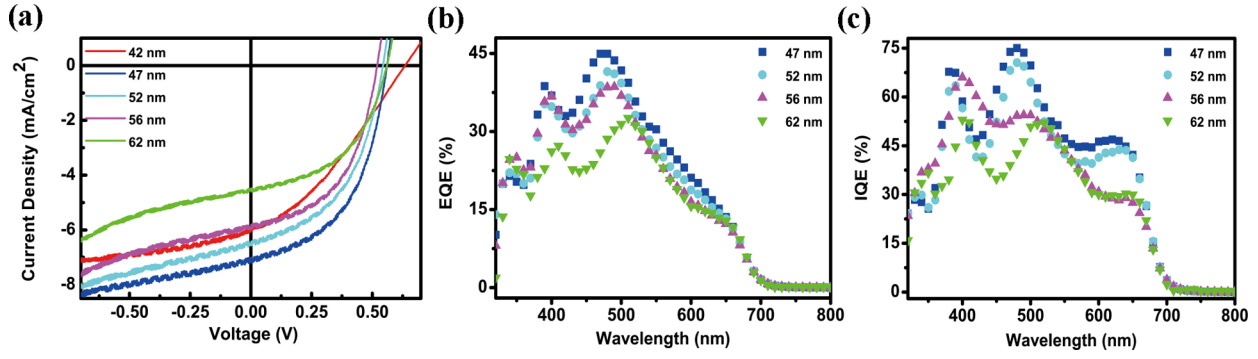

Figure 2. Single-junction P3HT:CdSe nanocrystal BHJ hybrid solar cell performance with different active layer thicknesses. (a) $I-V$ curves. (b) External quantum efficiency spectra. (c) Internal quantum efficiency spectra.

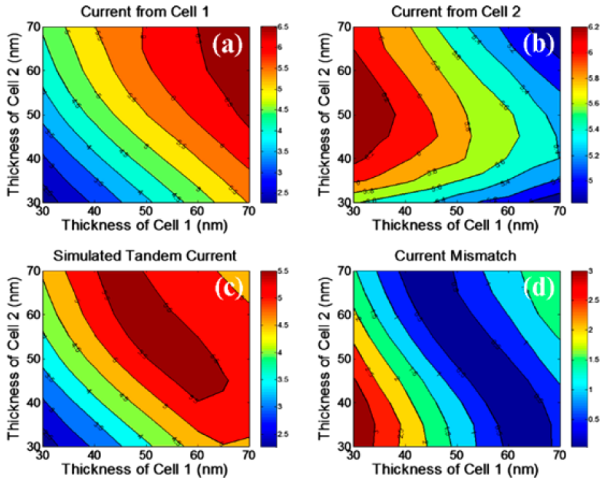

Figure 3. (a) Simulated photocurrent from cell 1 in the tandem device as a function of active layer thickness. (b) Simulated photocurrent from cell 2 in the tandem device as a function of active layer thickness. (c) Photocurrent for the tandem device taken from the lowest photocurrent of the two cells. (d) Current mismatch calculated from the difference in photocurrent between cell 1 and cell 2.

reflective aluminum contact, it is necessary to carefully control the thickness of the individual subcells so that they are positioned in locations with maximized optical field intensity. The importance of this behavior is reflected in the simulated photocurrent for cell 2 (Figure 3b), where, for a given thickness for cell 1, the highest photocurrent is not achieved for the thickest cell 2 but instead occurs at intermediate thickness where the cell encounters a maximum in optical field strength. These results affirm that the ideal tandem device would contain cells that are optimized for optical field intensity and not simply the largest thickness attainable.

Additionally, because the two cells are connected in series where electrons produced from the front subcell and holes produced from the rear subcell are recombined in the interconnecting layer, the extractable photocurrent of the tandem hybrid solar cell is limited by the individual cell with the smallest photocurrent. It is therefore important to balance the photocurrent of the two cells to improve the total device efficiency. This is illustrated in Figures 3c and 3d, which show the simulated photocurrent for the tandem device and the photocurrent mismatch between the two cells, respectively. These results highlight that the overall tandem performance is maximized at intermediate thicknesses. On the basis of these simulations, the optimal tandem performance should be achieved for individual subcell thicknesses around 50−60 nm.

Experimentally, the thicknesses of both the front (1) and rear (2) active layers were independently tuned from 47 to 62 nm. The details of the device performance for these tandem hybrid solar cells are summarized in Table S1 (Supporting Information). The best performing tandem hybrid solar cell has a front active layer thickness of 47 nm and a rear active layer thickness of 52 nm, which is in close agreement with the results of the simulation (vide supra). The champion tandem hybrid solar cells give J_{SC} = 5.04 mA cm^{-2}, V_{OC} = 1.33 V, FF = 0.47, and PCE = 3.12%. On average from 10 to 16 devices over four separate substrates, the optimized tandem hybrid solar cells exhibit J_{SC} = 4.61(0.39) mA cm^{-2}, V_{OC} = 1.28(0.05) V, FF = 0.46(0.02), and PCE = 2.7(0.28)%. Surprisingly, the measured average V_{OC} (1.28 V) is 2.25 times that of the average for an optimized single-junction device. This is a result of higher shunt resistance in tandem devices, which in turn decreases the dark current (J_0) in the tandem device. Figure 4

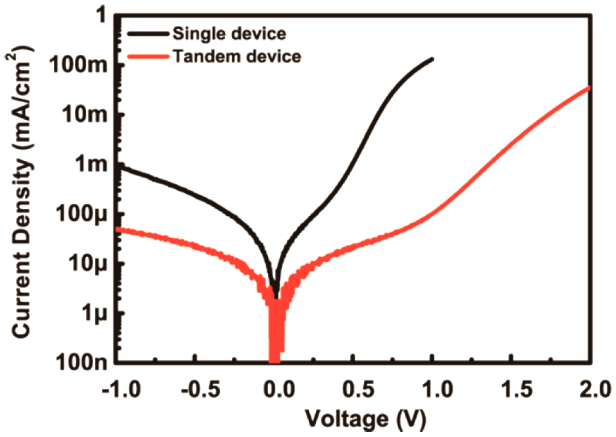

Figure 4. Dark $I-V$ characteristic of single-junction and tandem P3HT:CdSe hybrid solar cells.

shows the dark current of both the single-junction device and tandem device. The dark current of the tandem device at −1 V (0.05 mA cm^{-2}) is 1/20th of that of the single-junction device (1 mA cm^{-2}). On the basis of the diode equation, it is expected that lower dark current would lead to higher V_{OC}.

We also note that neither the V_{OC} nor FF change significantly in the tandem hybrid solar cells with different active layer thickness combinations; however, J_{SC} does change dramatically with the different active layer thickness combinations. To understand this effect, it is critical to point out that the maximum J_{SC} of a tandem solar cell connected in series is limited by the subcell that produces the smallest amount of photocurrent.[25] As such, individual subcells should be designed to produce matched photocurrents, thereby maximizing the efficiency of extracting photogenerated charge carriers. To ensure enough light absorption in the rear cell, the thicknesses of rear cells are designed to be greater than or equal to that of the front cell. Following this design criteria in our optimized tandem hybrid cell, we observe an average J_{SC} = 4.61(0.39) mA cm^{-2}. Assuming the front and rear subcells have a matched photocurrent, the sum of the J_{SC} values from the two subcells in the optimal tandem device is around 9.22 mA cm^{-2}, which is significantly higher than 6.95 mA cm^{-2} obtained from the optimized single-junction device. To understand this photoresponse observed in our system, the absorption of both the optimized single-junction and tandem hybrid P3HT:CdSe solar cells was measured in an integrating sphere in reflectance mode (Figure 5). From these results, it is clear that the absorption in the region of 480−600 nm in the tandem device is increased from 60% to 80% relative to the single-junction device, thereby demonstrating that the tandem configuration with two identical subcells does indeed improve light harvesting and lead to higher photoresponse than expected.

B.3. Triple-Junction Hybrid P3HT:CdSe Solar Cells. As a general proof of principle, triple-junction tandem hybrid solar cells were also fabricated with three identical P3HT:CdSe nanocrystal BHJ active layers, and the resulting devices exhibited a more than 3-fold increase in V_{OC} (V_{OC} = 1.91(0.20) V) relative to the single-junction device. The $I-V$ curves of the optimized champion hybrid solar cells with single-

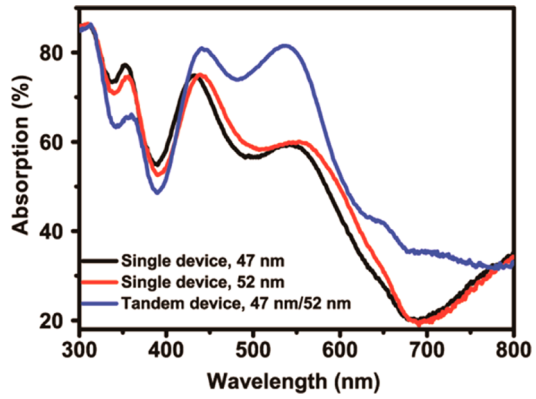

Figure 5. Double-pass absorption percentage of single-junction and tandem P3HT:CdSe hybrid solar cells.

junction, double-junction, and triple-junction device geometries are given in Figure 6, and the device parameters are

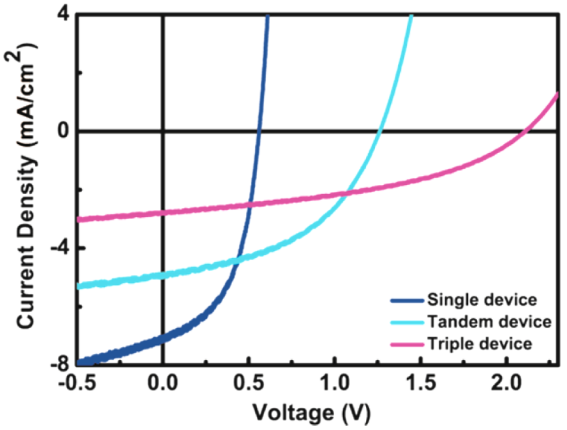

Figure 6. $I-V$ curves of P3HT:CdSe single-junction (47 nm active layer), tandem (47/52 nm), and triple-junction (47/47/56 nm) hybrid solar cells.

summarized in Table 2. The thicknesses of the active layers in the triple-junction hybrid solar cells were 47, 47, and 56 nm (from front to rear relative to incident irradiation). The average PCE of the triple-junction devices (η_P = 2.3%) is not higher than the double-junction devices because the thicknesses of each subcell were not optimized to give the best current; however, the open-circuit potential was shown to be additive from those of the three subcells as expected for a triple-junction device connected in series. Therefore, the combination of nanocrystalline ZnO and pH-neutral PEDOT:PSS is a robust ICL for serial multijunction hybrid solar cells.

IV. CONCLUSIONS

We present the first successful example of tandem and triple-junction hybrid polymer:nanocrystal solar cells with identical subcells based on P3HT:CdSe nanocrystal BHJs. The tandem hybrid solar cells give a 2-fold increase in V_{OC} over that of single-junction devices, and light absorption in the region of 480−600 nm is increased from 60% to 80% compared to the single-junction hybrid solar cells. To further prove the robustness of this device architecture, triple-junction hybrid solar cells were also fabricated and were shown to produce three times the V_{OC} of single-junction devices. The PCE exhibits a substantial increase from 2.0% in single-junction devices to 2.7% (champion 3.1%) in tandem devices and 2.3% in triple-junction devices. The results clearly indicate that tandem/multijunction device geometries are an effective approach to harvest more light and improve PCE in hybrid BHJ solar cells. This may be further extended to multijunction hybrid devices containing nonequivalent subcells with complementary absorption from both the selection of polymers and the composition and/or size of quantum dots with different band gaps, which offers additional parameter space for device optimization.

■ ASSOCIATED CONTENT

Supporting Information

Details of synthesis and ligand exchange process of CdSe nanocrystals, photovoltaic performance of tandem hybrid solar cell with different thicknesses, and absorption percentage of single junctions. This material is available free of charge via the Internet at http://pubs.acs.org.

■ AUTHOR INFORMATION

Corresponding Author

*E-mail: brutchey@usc.edu.

Notes

The authors declare no competing financial interest.

■ ACKNOWLEDGMENTS

This work was supported as part of the Center for Energy Nanoscience, an Energy Frontier Research Center funded by the U.S. Department of Energy, Office of Science, Office of Basic Energy Sciences under Award Number DE-SC0001013.

■ REFERENCES

(1) Milliron, D. J.; Gur, I.; Alivisatos, A. P. Hybrid Organic−Nanocrystal Solar Cells. *MRS Bull.* **2005**, *30*, 41−44.
(2) McGehee, M. D. Nanostructured Organic−Inorganic Hybrid Solar Cells. *MRS Bull.* **2009**, *34*, 95−100.
(3) Huynh, W. U.; Dittmer, J. J.; Alivisatos, A. P. Hybrid Nanorod-Polymer Solar Cells. *Science* **2002**, *295*, 2425−2427.

Table 2. Photovoltaic Device Details for Optimized Single-Junction, Tandem, and Triple-Junction Hybrid Solar Cells Based on a P3HT:CdSe BHJ[a]

devices	J_{SC} (mA cm^{-2})	V_{OC} (V)	FF	PCE (%)
single device[b]	6.95 ± 0.33	0.57 ± 0.01	0.50 ± 0.01	1.98 ± 0.12
tandem device[c]	4.61 ± 0.39	1.28 ± 0.05	0.46 ± 0.02	2.70 ± 0.29
triple device[d]	2.80 ± 0.14	1.91 ± 0.20	0.42 ± 0.02	2.26 ± 0.28
champion tandem device	5.04	1.33	0.47	3.12

[a]The device parameters were measured under AM 1.5G illumination at 1 sun. Average numbers and the associated standard deviations were determined over a total of 10−16 devices over four separate substrates. [b]Active layer thickness is 47 nm. [c]Active layer thicknesses are 47 nm (front) and 52 nm (rear). [d]Active layer thicknesses are 47 nm (front), 47 nm (middle), and 56 nm (rear).

(4) Borchert, H. Elementary Processes and Limiting Factors in Hybrid Polymer/Nanoparticle Solar Cells. *Energy Environ. Sci.* **2010**, *3*, 1682.
(5) Ren, S.; Chang, L. Y.; Lim, S. K.; Zhao, J.; Smith, M.; Zhao, N.; Bulovic, V.; Bawendi, M.; Gradecak, S. Inorganic-Organic Hybrid Solar Cell: Bridging Quantum Dots to Conjugated Polymer Nanowires. *Nano Lett.* **2011**, *11*, 3998−4002.
(6) Zhou, R.; Stalder, R.; Xie, D.; Cao, W.; Zheng, Y.; Yang, Y.; Plaisant, M.; Holloway, P. H.; Schanze, K. S.; Reynolds, J. R.; Xue, J. Enhancing the Efficiency of Solution-Processed Polymer:Colloidal Nanocrystal Hybrid Photovoltaic Cells Using Ethanedithiol Treatment. *ACS Nano* **2013**, *7*, 4846−4854.
(7) Liu, Z.; Sun, Y.; Yuan, J.; Wei, H.; Huang, X.; Han, L.; Wang, W.; Wang, H.; Ma, W. High-Efficiency Hybrid Solar Cells Based on Polymer/PbS_xSe_{1-x} Nanocrystals Benefiting From Vertical Phase Segregation. *Adv. Mater.* **2013**, *25*, 5772−5778.
(8) Greaney, M. J.; Araujo, J.; Burkhart, B.; Thompson, B. C.; Brutchey, R. L. Novel Semi-Random and Alternating Copolymer Hybrid Solar Cells Utilizing CdSe Multipods as Versatile Acceptors. *Chem. Commun.* **2013**, *49*, 8602−8604.
(9) Gur, I.; Fromer, N. A.; Chen, C.-P.; Kanaras, A. G.; Alivisatos, A. P. Hybrid Solar Cells with Prescribed Nanoscale Morphologies Based on Hyperbranched Semiconductor Nanocrystals. *Nano Lett.* **2006**, *7*, 409−414.
(10) Jeltsch, K. F.; Schädel, M.; Bonekamp, J.-B.; Niyamakom, P.; Rauscher, F.; Lademann, H. W. A.; Dumsch, I.; Allard, S.; Scherf, U.; Meerholz, K. Efficiency Enhanced Hybrid Solar Cells Using a Blend of Quantum Dots and Nanorods. *Adv. Funct. Mater.* **2012**, *22*, 397−404.
(11) Greaney, M. J.; Das, S.; Webber, D. H.; Bradforth, S. E.; Brutchey, R. L. Improving Open Circuit Potential in Hybrid P3HT:CdSe Bulk Heterojunction Solar Cells via Colloidal *tert*-Butylthiol Ligand Exchange. *ACS Nano* **2012**, *6*, 4222−4230.
(12) Lokteva, I.; Radychev, N.; Witt, F.; Borchert, H.; Parisi, Jr.; Kolny-Olesiak, J. Surface Treatment of CdSe Nanoparticles for Application in Hybrid Solar Cells: The Effect of Multiple Ligand Exchange with Pyridine. *J. Phys. Chem. C* **2010**, *114*, 12784−12791.
(13) Radychev, N.; Lokteva, I.; Witt, F.; Kolny-Olesiak, J.; Borchert, H.; Parisi, Jr. Physical Origin of the Impact of Different Nanocrystal Surface Modifications on the Performance of CdSe/P3HT Hybrid Solar Cells. *J. Phys. Chem. C* **2011**, *115*, 14111−14122.
(14) Greaney, M. J.; Brutchey, R. L. Ligand Engineering in Hybrid Polymer:Nanocrystal Solar Cells. *Mater. Today* **2014**, DOI: 10.1016/j.mattod.2014.07.004.
(15) Seo, J.; Cho, M. J.; Lee, D.; Cartwright, A. N.; Prasad, P. N. Efficient Heterojunction Photovoltaic Cell Utilizing Nanocomposites of Lead Sulfide Nanocrystals and a Low-Bandgap Polymer. *Adv. Mater.* **2011**, *23*, 3984−3988.
(16) Wu, Y.; Zhang, G. Performance Enhancement of Hybrid Solar Cells Through Chemical Vapor Annealing. *Nano Lett.* **2010**, *10*, 1628−1631.
(17) Couderc, E.; Greaney, M. J.; Brutchey, R. L.; Bradforth, S. E. Direct Spectroscopic Evidence of Ultrafast Electron Transfer from a Low Band Gap Polymer to CdSe Quantum Dots in Hybrid Photovoltaic Thin Films. *J. Am. Chem. Soc.* **2013**, *135*, 18418−18426.
(18) ten Cate, S.; Schins, J. M.; Siebbeles, L. D. A. Origin of Low Sensitizing Efficiency of Quantum Dots in Organic Solar Cells. *ACS Nano* **2012**, *6*, 8983−8988.
(19) Gao, F.; Li, Z.; Wang, J.; Rao, A.; Howard, I. A.; Abrusci, A.; Massip, S.; McNeill, C. R.; Greenham, N. C. Trap-Induced Losses in Hybrid Photovoltaics. *ACS Nano* **2014**, *8*, 3213−3221.
(20) Kim, J. Y.; Lee, K.; Coates, N. E.; Moses, D.; Nguyen, T.-Q.; Dante, M.; Heeger, A. J. Efficient Tandem Polymer Solar Cells Fabricated by All-Solution Processing. *Science* **2007**, *317*, 222−225.
(21) You, J.; Chen, C. C.; Hong, Z.; Yoshimura, K.; Ohya, K.; Xu, R.; Ye, S.; Gao, J.; Li, G.; Yang, Y. 10.2% Power Conversion Efficiency Polymer Tandem Solar Cells Consisting of Two Identical Sub-Cells. *Adv. Mater.* **2013**, *25*, 3973−3978.
(22) You, J.; Dou, L.; Yoshimura, K.; Kato, T.; Ohya, K.; Moriarty, T.; Emery, K.; Chen, C. C.; Gao, J.; Li, G.; Yang, Y. A Polymer Tandem Solar Cell with 10.6% Power Conversion Efficiency. *Nat. Commun.* **2013**, *4*, 1446.
(23) Zhang, C.; Tong, S. W.; Jiang, C.; Kang, E. T.; Chan, D. S. H.; Zhu, C. Simple Tandem Organic Photovoltaic Cells for Improved Energy Conversion Efficiency. *Appl. Phys. Lett.* **2008**, *92*, 083310.
(24) Dennler, G.; Scharber, M. C.; Ameri, T.; Denk, P.; Forberich, K.; Waldauf, C.; Brabec, C. J. Design Rules for Donors in Bulk-Heterojunction Tandem Solar Cells Towards 15% Energy-Conversion Efficiency. *Adv. Mater.* **2008**, *20*, 579−583.
(25) Ameri, T.; Dennler, G.; Lungenschmied, C.; Brabec, C. J. Organic Tandem Solar Cells: A Review. *Energy Environ. Sci.* **2009**, *2*, 347.
(26) Kaltenhauser, V.; Rath, T.; Edler, M.; Reichmann, A.; Trimmel, G. Exploring Polymer/Nanoparticle Hybrid Solar Cells in Tandem Architecture. *RSC Adv.* **2013**, *3*, 18643.
(27) Yu, W. W.; Qu, L.; Guo, W.; Peng, X. Experimental Determination of the Extinction Coefficient of CdTe, CdSe, and CdS Nanocrystals. *Chem. Mater.* **2003**, *15*, 2854−2860.
(28) Qian, L.; Yang, J.; Zhou, R.; Tang, A.; Zheng, Y.; Tseng, T.-K.; Bera, D.; Xue, J.; Holloway, P. H. Hybrid Polymer-CdSe Solar Cells with a ZnO Nanoparticle Buffer Layer for Improved Efficiency and Lifetime. *J. Mater. Chem.* **2011**, *21*, 3814−3817.
(29) Webber, D. H.; Brutchey, R. L. Ligand Exchange on Colloidal CdSe Nanocrystals Using Thermally Labile *tert*-Butylthiol for Improved Photocurrent in Nanocrystal Films. *J. Am. Chem. Soc.* **2012**, *134*, 1085−1092.
(30) Li, W.; Furlan, A.; Hendriks, K. H.; Wienk, M. M.; Janssen, R. A. Efficient Tandem and Triple-Junction Polymer Solar Cells. *J. Am. Chem. Soc.* **2013**, *135*, 5529−5532.
(31) Gilot, J.; Wienk, M. M.; Janssen, R. A. J. Double and Triple Junction Polymer Solar Cells Processed from Solution. *Appl. Phys. Lett.* **2007**, *90*, 143512.
(32) Pettersson, L. A. A.; Roman, L. S.; Inganäs, O. Modeling Photocurrent Action Spectra of Photovoltaic Devices Based on Organic Thin Films. *J. Appl. Phys.* **1999**, *86*, 487−496.